

Electrical transport in the lanthanum and erbium cobaltites

(Review Article)

Yu.N. Chiang and M.O. Dzyuba

*B. Verkin Institute for Low Temperature Physics and Engineering of the National Academy of Sciences of Ukraine
47 Nauky Ave., Kharkiv 61103, Ukraine*

E-mail: dzyuba@ilt.kharkov.ua

Received August 16, 2018, revised January 30, 2020, published online April 24, 2020

The review is devoted to the conductive properties of the multielement compounds such as lanthanum and erbium cobaltites. These properties are associated with a dopant-controlled interaction of the delocalized electrons with the local magnetic moments. It is considered the basic physical mechanisms that determine the transport properties of perovskitelike materials. It is given main experimental results for lanthanum and erbium cobaltites, and it is considered the influence of the polycrystallinity factor of samples on their galvanomagnetic properties.

Keywords: granulated cobaltite, magnetoresistance, double exchange, spin-polarized tunneling.

Contents

1. Introduction.....	671
2. LaCoO_3 (LCO).....	672
3. $\text{La}_{1-x}\text{Sr}_x\text{CoO}_3$ (LSCO), $(\text{La}_{1-x}\text{Sr}_x)_{1-y}\text{Ag}_y\text{CoO}_3$ (LSACO), $\text{La}_{1-y}\text{Ag}_y\text{CoO}_3$ (LACO).....	673
4. $\text{Er}_{1-x}\text{Sr}_x\text{CoO}_3$ (ESCO).....	677
5. Conclusion	679
References.....	679

1. Introduction

A large class of compounds with strong electron correlations (SEC) includes materials based on transition metals with incomplete d or f atomic orbitals. The strong localization of these orbitals in space leads to a significant interaction between electrons, in contrast with the case of s or p electrons, and the inapplicability of the approach of free electrons. The interaction of the spin, charge, and orbital momentum of d or f electrons in such materials makes them extremely sensitive to external influences such as temperature, magnetic field, pressure, or doping. This leads to the appearance in such compounds of unique electronic and magnetic properties. The most well-known and studied effects in the compounds with SEC are the effect of a colossal magnetoresistance in manganites [1] and the high-temperature superconductivity in cuprates [2]. However, these are not all intriguing phenomena that are observed in the strongly correlated systems; in addition to the above, one can distinguish the following effects: the metal-insulator

transition [3], charge ordering [4], phase separation [5–7], ferroelectricity [8] and others. At the same time the polycrystallinity of the samples, which is typical for granular composites such as ceramics, plays a role in the appearance of these effects [9,10]. In general, the mechanisms of transport of charge carriers in materials with SEC can be divided into two types — intragranular mechanisms of electron correlation and intergranular tunneling mechanisms [10], which leads to a mixed or hybrid conductivity. Since most of the multicomponent compounds are synthesized in the form of granular ceramics, the important task for practical application is to find out the mechanisms of intergranular tunneling and influence the geometric and spatial parameters of crystallites to these mechanisms. Such variety of phenomena in materials with SEC has already led to a numerous technological solutions, and there is no doubt about success of their further application in science and technology.

Like in other perovskites electronic and magnetic properties of the cobaltites are determined by Co–O–Co bonding.

However, the doping cation affects inclination and rotation of the octahedron CoO_6 , and any deviation of the Co-O-Co of 180° reduces the probability of carrying the e_g electron and the width of the conductivity zone. In the case of the SrCoO_3 compound, the crystal structure is cubic, and the Co-O-Co bond angle is 180° . Accordingly, this compound exhibits a metal behavior up to the lowest temperatures [11]. The reduction of the doping ion radius distorts the lattice and changes symmetry from cubic to rhombohedral or orthorhombic with corresponding reduction of the Co-O-Co bond angle [12]. This takes place in the ReCoO_3 compounds, where Re is a trivalent rare-earth element. In those compounds the metal-insulator transition is observed at the temperature which depends on the radius of cation Re [13]. The one of the latest reviews dedicated to the different properties of the cobaltites is written by B. Reveau and M.M. Seikh [14].

2. LaCoO_3 (LCO)

LaCoO_3 as the initial compound of the group $\text{La}_{1-x}\text{Sr}_x\text{CoO}_3$ is typical broadband cobaltite. The crystal structure of this compound is a distorted perovskite lattice with a rhombohedral symmetry ($R\bar{3}c$) at 300 K. The rhombohedral distortion arises due to the cooperative rotation and compression of the octahedron CoO_6 along the axis [111] through the displacement of the oxygen atoms. It should be noted that the structural distortion decreases with a temperature increasing, and above 1610 K, the lattice becomes cubic [15].

Measurement of the bond gap in LaCoO_3 is conflicting, various experimental techniques yield different results [16]. However, it was reported that in LaCoO_3 an optical gap for carrying charge $\sim 100\text{--}200$ meV, and a spin gap, which is defined as the difference between splitting by crystal field

and Hund's exchange $\sim 10\text{--}80$ meV [16–19]. As a result, at 0 K, all of the Co ions are in the low-spin state ($t_{2g}^6 e_g^0$), and LaCoO_3 is a diamagnetic insulator ($\rho > 10^9$ Ohm·cm) [20]. When the temperature rises above 30 K, the thermal energy transfers some of the t_{2g} electrons to the e_g level and the ions of Co are transferred to a higher spin state with a magnetic moment. This spin transition occurs in the temperature range from 30 to 100 K, and manifests itself as an increase in the magnetic susceptibility in this temperature range (Fig. 1(a)). However, despite the fact that above 100 K Co ions have a magnetic moment, the long-range magnetic order is not observed, and the susceptibility corresponds to the paramagnetic Curie–Weiss behavior. In addition, in the low-spin state, LaCoO_3 should exhibit a weak diamagnetic response ($\chi < 0$), but the experiment shows an increase in magnetic susceptibility when the temperature is lower than 30 K (Fig. 1(a)). This behavior was explained by surface effects [21,22], local moments of oxygen vacancies [23] or other impurities. With regard to electronic transport, LaCoO_3 remains a semiconductor up to a temperature of 500 K, at which the insulator-metal transition takes place (Fig. 1(a)). The high-temperature metallic ground state is due to an increase in the amount of delocalized charge carriers and the closure of the charge gap, which is similar to the case of hole doping [24]. The last investigations indicates the symmetry change in the Co $3d$ electron-orbital states at around 500 K, which reveals the electron transfer from t_{2g} to e_g orbitals similar to that of the spin crossover around 100 K. The magnitude of the difference Compton profiles exhibits a steep increase at 500 K, implying a cooperative character of the 500-K spin-crossover phenomenon. The difference Compton profiles show an increment of the characteristics of hybridization between Co $3d$ and O $2p$ orbitals, which suggests the development

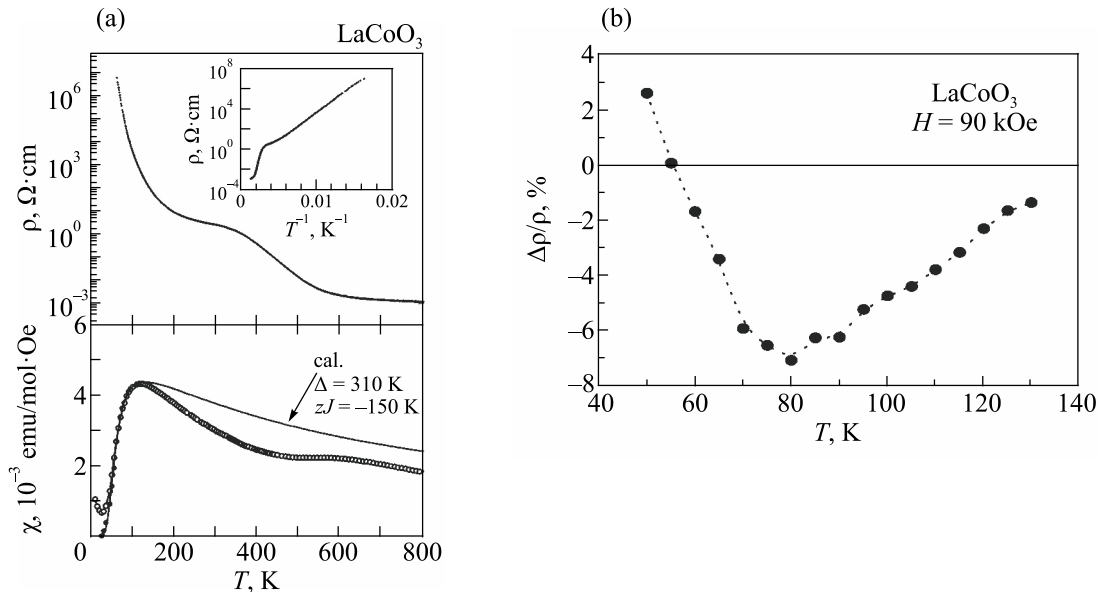


Fig. 1. (a) Temperature dependence of the specific resistance of the LaCoO_3 single crystal (top panel). Magnetic susceptibility of the same sample (lower panel) [19]. (b) The peak of the negative magnetoresistance at 80 K in the LaCoO_3 polycrystalline sample [26].

of the molecular orbital formation [25]. The metal-insulator transition corresponds to the plateau depending of the magnetic susceptibility on the temperature, and the metallic state again obeys the Curie–Weiss law (Fig. 1(a)). Despite the fact that spin transition is clearly observed in the range of 30–100 K on the magnetic susceptibility curve, it is not so pronounced in transport measurements, correlating only with the peak of a magnetoresistance at 80 K in the field 9 T, which is due to the inhibition of dispersion by strong magnetic field at the spin disorder (Fig. 1(b)) [26].

3. $\text{La}_{1-x}\text{Sr}_x\text{CoO}_3$ (LSCO), $(\text{La}_{1-x}\text{Sr}_x)_{1-y}\text{Ag}_y\text{CoO}_3$ (LSACO), $\text{La}_{1-y}\text{Ag}_y\text{CoO}_3$ (LACO)

The introduction of Sr in the LaCoO_3 lattice greatly affects its properties, both structural and electronic. The ion radius Sr^{2+} is greater than the ion radius La^{3+} , so the average radius of the doping ion increases, while decreasing the rhomboidric distortion of the lattice. For $x = 0.5$ the rhombohedral symmetry changes by cubic $Pm\bar{3}m$ at 300 K. This results in a change in the Co–O–Co coupling angle to 180° [27]. Effectively doping with strontium reduces the transition temperature from the rhombohedral symmetry to the cubic symmetry from 1610 K to 300 K.

The effect of doping with strontium on electrical properties is slightly more complicated. The replacement of trivalent lanthanum with divalent strontium converts the corresponding amount of Co^{3+} into the Co^{4+} state and introduces a hole in the system. Within one of the models, it is assumed that Co^{4+} , through a smaller ion radius, draws neighboring oxygen ions, which in turn leads to the disappearance of the spin gap in the nearest Co^{3+} ions, contributing to the Jahn-Teller stabilization of the intermediate spin state (ISS), while the Co^{4+} ions remain in the low spin state (LSS). The double exchange between the ISS Co^{3+} and LSS Co^{4+} ions, which differ in $1 e_g$ electron, delocalizes a e_g hole within these seven ions, thus creating a magnetic polaron with a large spin quantum number [19,28–31]. Yamaguchi *et al.* reported a large spin of this polaron $S = 10\text{--}16$, indicating the possibility of the existence of a high spin state (HSS) [19]. In light doping conditions ($x = 0.04$), these spin polarons remain isolated and weakly interact, but they are noticeably manifested in the low-temperature part of the susceptibility, in which a paramagnetic contribution appears below 100 K [19]. Experiments on the elastic neutron scattering [30,31] suggest the presence of such polarons. It should be noted that this does not mean the complete disappearance of the spin transition — the LSS ions still exist in the unperturbed region. Most likely, their weak diamagnetic signal is invisible in the background of a much larger paramagnetic moment of ions in the ISS. Schematically, such magnetic polaron is depicted in Fig. 2(a) [29], and its influence on the susceptibility of weakly doped compounds is shown in Fig. 2(b) [19]. Sev-

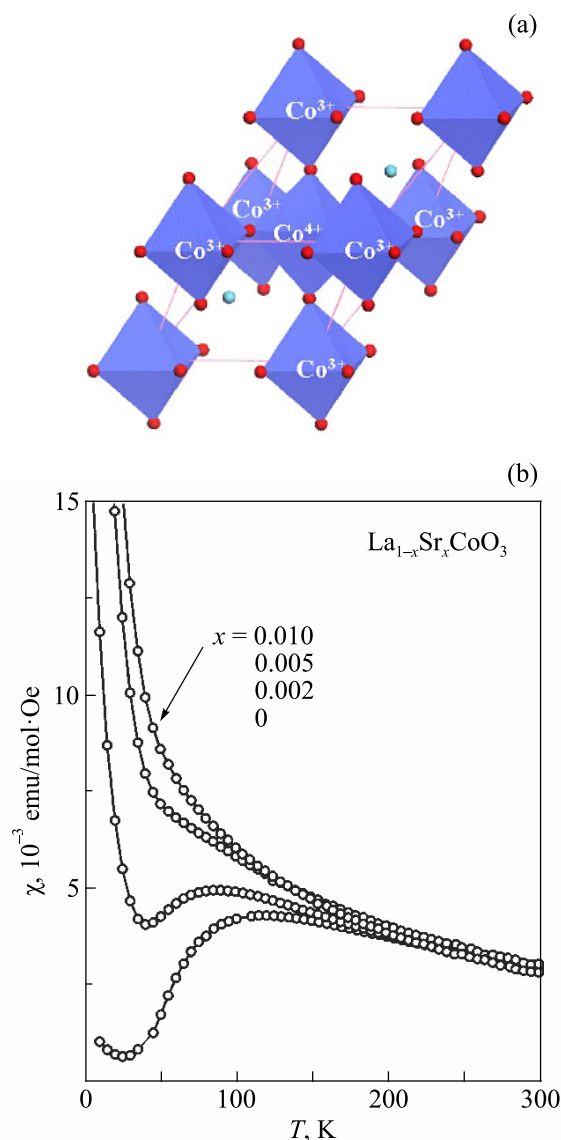


Fig. 2. (a) The schematic representation of the magnetic polaron detected in $\text{La}_{1-x}\text{Sr}_x\text{CoO}_3$ with weak doping [29]. (b) The magnetic susceptibility of weakly-doped crystals $\text{La}_{1-x}\text{Sr}_x\text{CoO}_3$ exhibits inhibition of the low-temperature fall of susceptibility [19].

eral models were proposed to describe such system (e.g., [32]), and qualitatively they all separate material on ferromagnetic metallic and non-ferromagnetic insulating regions with the existence of percolation above a certain critical level of doping.

When doping with strontium exceeds the critical value of $x = 0.04$, the polaron density becomes quite high for their integration and the formation of ferromagnetic cluster enriched with holes. These clusters are in an isolating matrix, which, nonetheless, contains separate polarons and a mixture of ISS Co^{3+} /LSS Co^{4+} . Such a phase separation into ferromagnetic clusters and a nonferromagnetic matrix is independently confirmed by methods of small-angle neutron scattering [33], nuclear magnetic resonance [34–37], inelastic neutron scattering [29,38] and electron spin resonance [30]. In practice, the phase separation in electrical transport

manifests itself as an intracluster giant magnetoresistance [39]. Usually, metals with a long-range ferromagnetic order exhibit an anisotropic magnetoresistance, which changes the sign when the angle between the transport current and the applied magnetic field is changed [40]. In the system $\text{La}_{1-x}\text{Sr}_x\text{CoO}_3$ with phase separation and isolated ferromagnetic clusters, electrical transport is carried out by means of jumps between clusters. This conductivity is maximal with the parallel orientation of the spins of all clusters and minimal at random orientation of spins. This leads to a large negative isotropic magnetoresistance in strong magnetic fields, which is similar to the effect of the giant magnetoresistance, which is observed in artificially created multilayers and granular metals [41–45]. Figure 3 illustrates spin-disordered $\text{La}_{1-x}\text{Sr}_x\text{CoO}_3$ clusters in the phase separated mode and an example of a giant magnetoresistance in a single crystal $\text{La}_{1-x}\text{Sr}_x\text{CoO}_3$ with $x = 0.15$ [39].

With increasing x , clusters increase in size, and for a critical value of $x = 0.18$ there is a sufficient overlapping between them to form a percolation grid through the entire material. At this point, in spite of the fact that the phase sep-

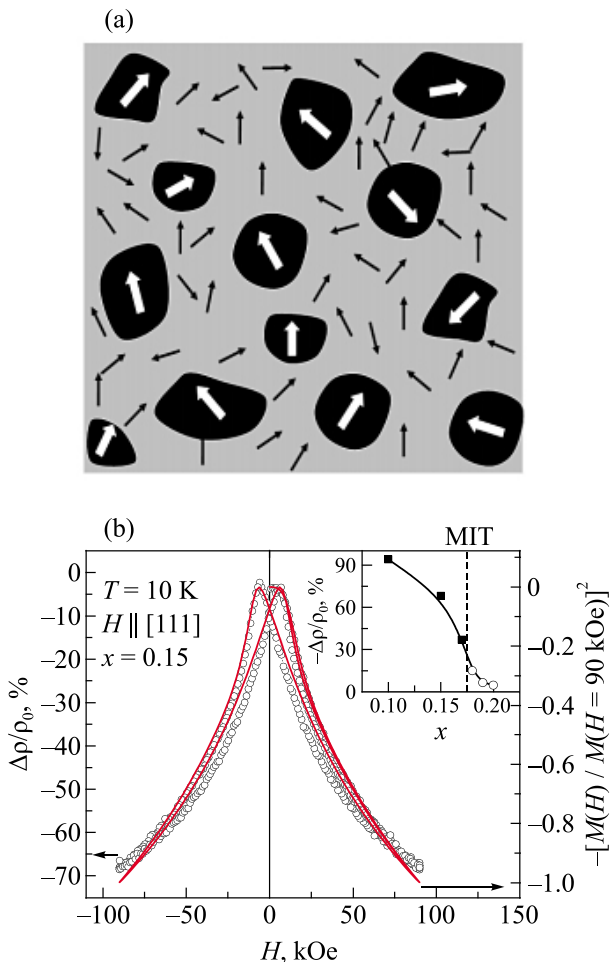


Fig. 3. (a) Illustration of spin-disordered cluster state $\text{La}_{1-x}\text{Sr}_x\text{CoO}_3$. (b) Giant negative magnetoresistance of $\text{La}_{1-x}\text{Sr}_x\text{CoO}_3$ single crystal with doping level $x = 0.15$. The insert shows the evolution of the magnetoresistance with an increase in the level of doping [39].

aration remains, in $\text{La}_{1-x}\text{Sr}_x\text{CoO}_3$ there is an insulator-metal transition and the material begins to behave like a ferromagnetic metal. The phase separation in the metallic state is confirmed by nuclear magnetic resonance [30,46]. The phase separation exists up to $x = 0.22$, at which the material becomes a homogeneous ferromagnetic metal. However, in polycrystals above $x = 0.22$, the non-ferromagnetic regions are observed by the method of nuclear magnetic resonance, and are explained by non-stoichiometry of the grain boundaries. As temperature rises, the long-range ferromagnetism evolves into ferromagnetic clusters of small size, with subsequent transition to a homogeneous paramagnetic state [47].

The experimental data presented above are in good agreement with the NMR ^{139}La studies [48]. In Fig. 4 it is shown the phase diagram of the $\text{La}_{1-x}\text{Sr}_x\text{CoO}_3$ system from [49].

The properties of granular systems may differ, and sometimes radically, from the properties of single crystals of the same composition. For example, polycrystals of ferromagnetic materials such as $\text{La}_{0.7}\text{Sr}_{0.3}\text{MnO}_3$, CrO_2 , Fe_2O_3 , exhibit a large magnetoresistive effect in small magnetic fields below the ferromagnetic transition temperature. At the same time, under the same conditions, the magnetoresistance of single crystals is much smaller or nonexistent [50–53]. It is clear from this fact that the giant magnetoresistance in such systems is the result of the granular nature of the samples. And, consequently, it should depend on the geometric and spatial factors of the internal structure, such as the size of the particles, their shape, the density of the packaging (porosity), etc.

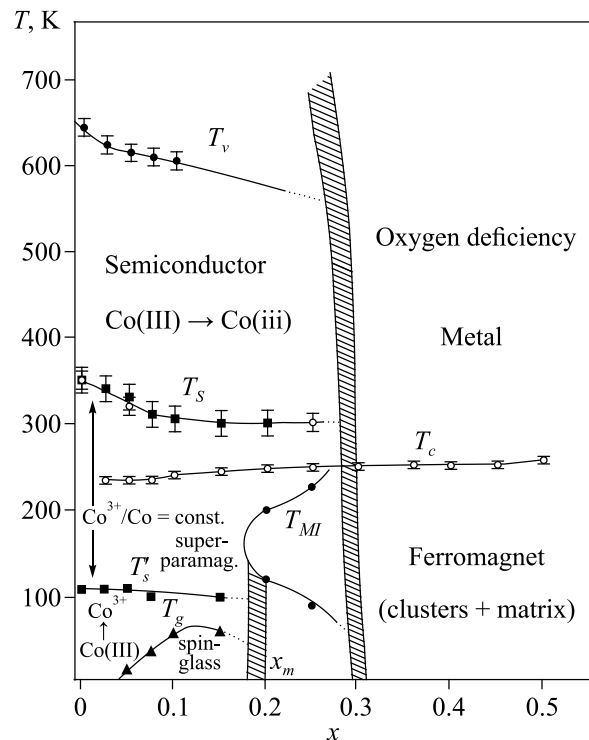


Fig. 4. The phase diagram of the $\text{La}_{1-x}\text{Sr}_x\text{CoO}_3$ system from [49].

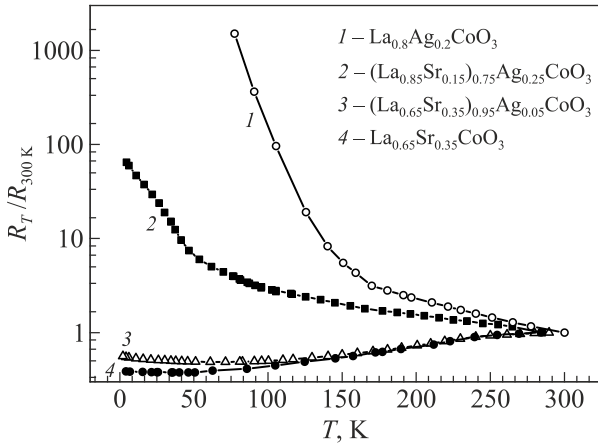


Fig. 5. Resistance of the hole-doped cobaltites, normalized to the resistance at 300 K, depending on the temperature [54,55].

In Fig. 5 it is shown the temperature dependencies of the resistance of samples of lanthanum cobaltites LACO, LSACO and LSCO differently doped with strontium and silver (dopant concentrations are shown in the figure). It can be seen that the hole doping with strontium, and not silver, radically changes the conductivity of undoped perovskite cobaltite LCO, which typically shows semiconductor temperature behavior, similar to the behavior of curve 1. Thus, by comparing curves 1 and 2, we see that for approximately equal concentration of silver a samples resistance varies greatly when strontium is introduced. For example, at $T \approx 100$ K, the resistance R_T of the samples with similar geometric parameters varies almost 10^4 times, and in units R_T/R_{300K} — 10^2 times.

Moreover, the decreasing in amount of silver which would have increase the resistance of the samples, only an increasing in the quantity of strontium deepens the metallic behavior of conductivity. It is observed over almost the entire temperature range below 300 K except the low temperatures (30–60 K), where minimum appears — the transition to nonmetal behavior. Apparently, this is confirmation of the insignificant role of silver electrons in exchange processes involving oxygen ions, possibly due to significant activation energies, which are confirmed by weak reactive and oxidative abilities of this element, at least in the composites of the chemical composition under consideration. Thus, the work [56] is point out to the high stability of Ag towards formation of Ag doped oxides upon solid-state synthesis from Ag and oxide precursors.

It should be noted that the transition from metal to nonmetal behavior was observed in massive granulated samples of the cobaltite LSCO with grain size $1 \mu\text{m}$ (Fig. 6). In the similar composition samples, but with the grain size of about $50 \mu\text{m}$, those minimum is not detected [57]. This indicates that the effect is due not so much to the hole doping level, but to the structural features, such as size and density of grain distribution.

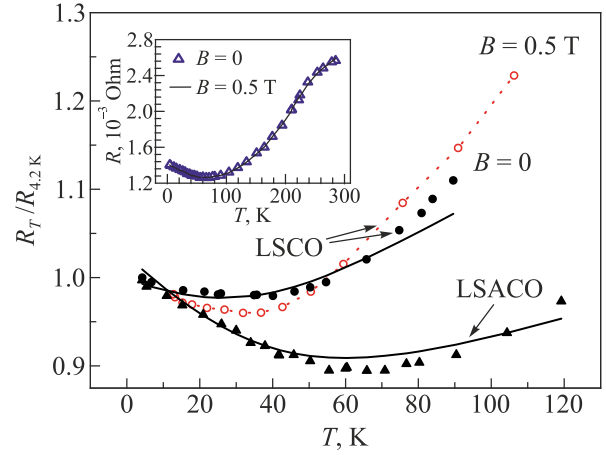


Fig. 6. Minimum on the temperature dependence of a normalized resistance of the hole-doped cobaltites LSCO and LSACO at level of lanthanum substitution by a strontium $x \approx 0.35$ at $B = 0$ and $B = 0.5$ T. On the insert — temperature dependence of the LSACO resistance [54,55].

In Fig. 6 it is shown the low temperature part of the curves with a transition from metal to nonmetal behavior of the conductivity. The minimum on the dependencies $R(T)$ means existence in the corresponding temperature range the competing mechanisms of the electron correlations with comparable in magnitudes contributions to the conductivity. This allows to conduct not only qualitative, but also quantitative analysis of the nature of the observed minimum, since it facilitates the self-matching of parameters that are used to describe the experiment by competing theoretical models.

The concept of two contributions to conductivity — intra- and intergranular — is chosen. The complete resistance of the system, normalized to the resistance of the sample at $T = T^*$, is represented as

$$\langle R(T) \rangle / \langle R(T^*) \rangle = \left[G_g^{-1} + G_{ISPT}^{-1} \right]_T / \langle \rho_{T^*} \rangle, \quad (1)$$

$$G_{g;ISPT} = \langle \sigma_{g;ISPT} \rangle$$

where G is the conductance as averaged over granular ensembles corresponding intragranular (G_g) and intergranular (G_{ISPT}) contributions to the specific conductivity σ (the angle brackets mean averaging), ρ_{T^*} — specific resistance at normalizing temperatures $T^* = 4.2$ and 300 K.

The systems (Re)SCO (Re — trivalent rare-earth element) can be represented as two-phase electronic systems [10]. The conductivity of one of the phases, the matrix (Re)CO, can be characterized by the thermoactivation mechanism of the semiconductor type σ_{sm} (for example, the Mott mechanism), and the conductivity of the other phase, the sublattice SCO, σ_{DE} , by the mechanism of the double ferromagnetic exchange [58] between conduction electrons of the various valence ions of cobalt. It should be noted that direct observation of double exchange in ferromagnetic $\text{La}_{0.7}\text{Sr}_{0.3}\text{CoO}_3$ by broadband ellipsometry was

reported in [59], confirming that the double exchange plays a major role in the ferromagnetism of doped cobaltites. As a result, the intragranular contribution to the conductivity will be written as $\sigma_{\Sigma} = \sigma_{sm} + \sigma_{DE}$ and the conductance of the granule as a whole is written in the form

$$\sigma_{\Sigma} = \sigma_{sm} + \sigma_{DE} = \sigma(T_r) \exp(-\Delta/T) + (\alpha e^2 / ah)(T_C / T), \quad (2)$$

where $\alpha = |\text{Co}^{4+}| / |\text{Co}^{3+}|$ is the proportion of Co^{4+} ions, T_C is the Curie temperature, T_r — room temperature, a — lattice parameter, h — Planck constant.

A parallel contribution to the conductivity of a granular magnetic system can be introduced by the intrinsic intergranular mechanism based on the principle of intergranular spin-polarized tunneling (ISPT) [60,61]. This model assumes that for tunneling through the boundary between two granules with antiparallel magnetization an electron have to get over the potential barrier of the order of the exchange energy E_m . As a result, the probability of tunneling, and the intergranular conductivity, are reduced by the factor $\exp(-E_m/kT)$ in comparison with the case of the ferromagnetic orientation of the granules magnetization vectors. As shown in paper [62], the model assumes a sharp change in the conductivity already in small magnetic fields ~ 0.1 T, if the initial (in zero field) distribution of the directions of magnetization of the granules was random (paramagnetic). However, it is obvious that this effect would be absent if the distribution in the zero field was initially close to antiferromagnetic (AFM). As will be seen below (Fig. 8) the magnetic fields up to 10 T have practically no effect on the conductivity of the samples with $x = 0.35$, which suggests an antiferromagnetic interaction of the granular magnetization in the zero field in these samples. The indications for AFM exchange between granules are also in works [62–64].

In [62] the expression for the intergranular conductivity of two granules due to the tunneling of spin-polarized electrons have been obtained:

$$\sigma_{ISPT} \propto (1/2)(n_{\uparrow} + n_{\downarrow}) [1 + P^2 \cos \theta], \quad (3)$$

where the polarization coefficient $P = (n_{\uparrow} + n_{\downarrow}) / (n_{\uparrow} - n_{\downarrow})$; $n_{\downarrow}, n_{\uparrow}$ — the densities of states of electrons at the Fermi level with spin “up” and “down”, respectively. Expression (3) establishes the dependence of the intergranular conductivity on the angle θ between directions of magnetization of adjacent granules. Following the so-called n - n conductivity models (in the nearest neighbors), Eq. (3) was averaged on the magnitudes $\cos \theta$ and on the probabilities of tunneling between the two pairs of the nearest ones neighbors for the entire ensemble of granule systems, and also it was taken into account the temperature dependence of the probability of tunneling thermoactivated charge carriers and the AFM interaction of the granules [60,61,64–66]. It allows present intergranular management in the form of:

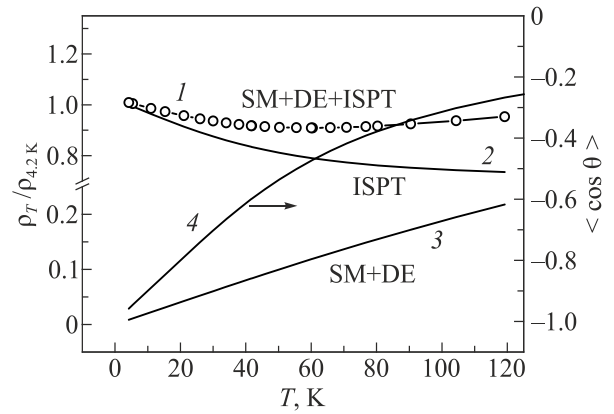


Fig. 7. Normalized resistance with minimum (open circles) and theoretical curve calculated by the formula (1) (solid line 1) for the sample LSACO ($x = 0.35, y = 0.05$). The intragranular contribution (curve 3) and the intergranular one (curve 2) are shown separately. Curve 4 is a spin correlation function for AFM interaction of the granules [54,55].

$$G_{ISPT} = \langle \sigma_{ISPT}(0 < T < T_C) \rangle = [\rho_{n-n}(U)]^{-1} [1 - P^2 \langle \cos \theta \rangle], \quad (4)$$

where angle brackets mean averaging; U — height of the intergranular potential barrier; $\rho_{n-n}(U) = \rho_0 + \beta T^{3/2}$ [66,67]; $\langle \cos \theta \rangle = \coth(J/T) - (J/T)^{-1}$ — spin correlation function $\langle \mathbf{S}_1 \cdot \mathbf{S}_2 \rangle$ [65,68]; J — exchange energy of AFM interaction; ρ_0 — residual resistive contribution of n - n interactions in the unactivated mode.

By combining Eqs. (2) and (4) in accordance with (1), it can be obtained the complete (normalized) impedance of the sample represented by solid curves in Fig. 7. Calculating these curves, it is considered that the temperature behavior of the intragranular conductivity can be quite general for the granular cobaltites. The comparison of the calculating and experimental data in the region of the resistance minimum for the studying samples (Figs. 7 and 8) gives grounds for

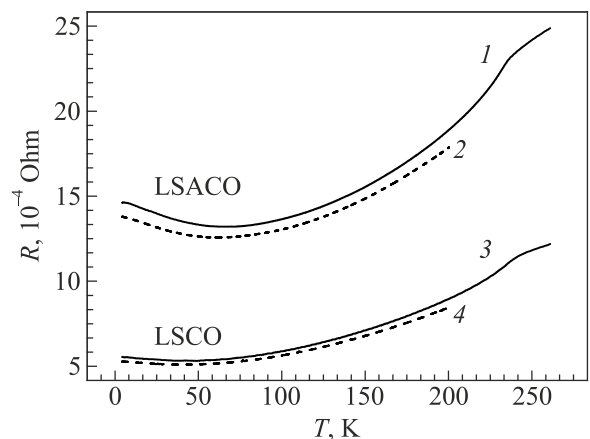


Fig. 8. Temperature dependencies of the resistance of samples with similar geometric sizes of cobaltites LSCO ($x = 0.35$) and LSACO ($x = 0.35, y = 0.05$) for $B = 0$ (curves 1 and 3) and in the applied magnetic field 10 T (curves 2 and 4) [55].

the conclusion that the proper conductivity of the granules in various samples with similar stoichiometry is determined by practically universal transfer mechanisms. At the same time, the position and depth of the minimum under these conditions depend mainly on the probability of intergranular tunneling, which is characterized by intergranular resistance ρ_{n-n} (U) that is, from the values ρ_0 and β . Although it was used ρ_{n-n} (U) in the form proposed in [66,67], at the end of the temperature interval with a minimum, the experimental curve exhibits a stronger temperature dependence ρ_{n-n} (U) than in the case of taking into account only the spin-wave term $T^{3/2}$. Perhaps this indicates the presence of a temperature dependence of the density imbalance of carrier states with different spins, which is not taken into account here. Thus, the two contributions concept reflected in the Eq. (2), not only qualitatively, but also with an acceptable accuracy, describes quantitatively the temperature behavior of the resistance of the cobaltites samples at $x = 0.35$ in the region of the minimum.

Figure 7 separately shows the own contribution of the granules (curve 3, SM + DE), the intergranular contribution (curve 2, ISPT) and the spin correlation function for AFM interaction of the granules (curve 4), by means of which curve 2 for LSACO compound was calculated, as well as the calculated total curve 1 (SM + DE + ISPT), passing through the experimental points.

The dependencies $R(T)$ of the ceramic cobaltites LSCO and LSACO samples in the external magnetic fields $B = 10$ T, as well as in the zero magnetic field are shown in Fig. 8. It can be seen that even the strong magnetic field practically does not change the position of the minimum, and the negative magnetoresistance does not exceed 6%. From the numerical calculations, it follows that the effective field $\cong 2\mu_B H / |J|$ with $B = 10$ T and $|J| / k_B \sim 100$ K is approximately 0.07. This is too low value to observe the difference between the temperature dependencies of conductance in the magnetic field and without it. A similar behavior was observed in manganites in the effective magnetic field up to 0.5 [64,65]. In other words, the energy of exchange interaction in cobaltites, which determines the AFM ordering at those temperatures where the resistance minimum is existing, is much greater than the magnetic energy in the 10 T field.

4. $\text{Er}_{1-x}\text{Sr}_x\text{CoO}_3$ (ESCO)

Erbium cobaltite (ESCO) synthesized by the standard three-phase technology confirmed the presence of polyhedral distortions of the cubic lattice, leading to the formation of an orthorhombically distorted structure of the type $Pbnm$ (prototype GdFeO_3). A similar structure was observed in cobaltites with gadolinium [69]. Basic the crystallographic unit — the octahedron CoO_6 — is rotated in the plane xy and inclined to the z axis. The presence in the perovskite structure of a rare earth ion with a reduced ion radius (in comparison with La) leads to the bending of Co-O-Co

coupling at an angle of 28° and a decrease in length Co-O bond, induced by reduced chemical pressure [70].

The study of the evolution of the electrical properties of erbium cobaltites in a wide range of concentrations of dopant Sr (from 0.25 to 0.99) allows us to qualitatively link the behavior of their conductivity to intragranular mechanisms. The experimentally observed temperature dependences of the specific resistance for the samples of almost all concentrations demonstrate a semiconductor behavior. An exception is only the sample $\text{Er}_{0.01}\text{Sr}_{0.99}\text{CoO}_{3-\delta}$, for which there is a narrow temperature range of the metallic behavior. Figure 9 shows the temperature dependencies of the specific resistance of the erbium cobaltites samples (ESCO) in a wide range of the concentration parameter x . As can be seen from this figure, the low-temperature behavior of the conductivity is substantially nonlinear and is closely related to the concentration of bivalent Sr. As in other cobaltites [71], the behavior of the conductivity of the presented samples does not correspond to the behavior of the conductivity of a single-phase system and, in particular, is not described by the Arrhenius function for a purely semiconductor system.

It is also evident that at high temperatures the temperature behavior of the conductivity is strongly, and also not monotonically depends on the concentration of doping cations (Fig. 10). As in the case of low temperatures, conductivity can not be described by one universal function, for example, only a function of the activation (hopping) type, which also testifies to the heterophasicity of the system and the explicit competition several types of the exchange interaction, one of which is indirect ferromagnetic coupling through conduction electrons, known as double exchange [58].

From curves in Figs. 9 and 10 it follows that the optimal conditions for the manifestation of the coupling of this type are realized in the range of concentrations $0.85 < x < 0.99$, in which the monotonic change in conductivity with the change in x is interrupted and a minimum resistance is achieved (at $x = 0.95$ with selected change step x).

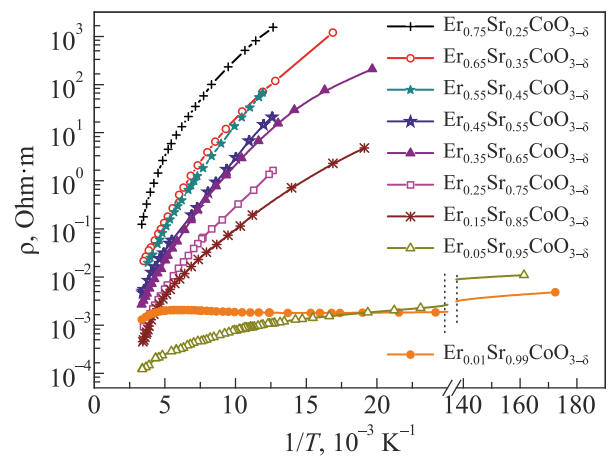


Fig. 9. Temperature dependences of the specific resistance of the ESCO samples in the wide range of the Sr concentration [72].

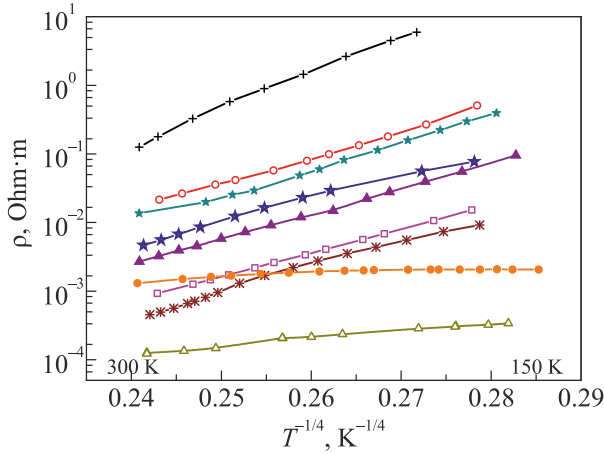


Fig. 10. High-temperature (T_r) behavior of the curves shown in Fig. 9, in the coordinates of Mott’s thermoactivated conductivity. Symbols for the corresponding x values are the same as in Fig. 9 [72].

In this concentration range, the conductivity is so far from the semiconductor that it allows it to be measured over a wide temperature range up to helium temperatures (up to 6 K), whereas for other concentrations it is not lower than 50 K. Figure 11 shows that at the upper edge of the indicated concentration interval, the temperature dependence of the conductivity $\sigma(1/T)$ acquires a nonmonotonic form: with the temperature decreasing, at $T \approx 150$ K the conductivity passes through the minimum, and at $T \approx 50$ K — through the maximum. In this connection, it can be assumed that in the discussed interval x , at least at low temperatures ($T < 50$ K), such anomalous behavior of the conductivity, indicating the presence of a metal-dielectric transition, must be associated with a rather high role of the double exchange mechanism, which competes with the direct antiferromagnetic exchange coupling between the magnetic moments of the d orbitals of cobalt ions.

Taking the concept of a two-phase system, the conductivity of the system can be presents as the sum of the con-

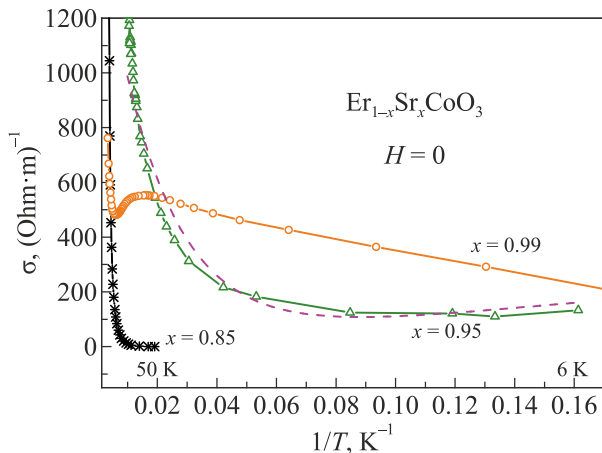


Fig. 11. The temperature behavior of the conductivity of the ESCO system in the concentration range $0.85 \leq x \leq 0.99$ [72].

tributions of the hopping mechanism (for example, Mott mechanism) and the double exchange mechanism, that is, in the form (2). In Fig. 11 it is shown the experimental values of conductivity as a function of inverse temperature for concentrations $0.85 \leq x \leq 0.99$ with a dashed curve describing the experimental data accordingly to the expression (2). The values of the fitting parameters are as follows: $a = 5.142 \text{ \AA}^{-1}$ [73]; $T_C = 160 \text{ K}$; $\Delta \approx 50 \text{ K}$; $\sigma(T_r) \approx 1600 \text{ (Ohm}\cdot\text{m)}^{-1}$; $(ae^2/ah)T_C \approx 1000 \text{ K/(Ohm}\cdot\text{m)}$. This expression describes well the temperature dependence of the conductivity at temperatures below 50 K for those concentrations where the double exchange is the most significant and the transition metal–isolator takes place. Also from this it follows that the proportion of Co^{4+} ions involved in the double exchange in order of magnitude is $\alpha \sim 10^{-4} - 10^{-5}$. Comparing the ratio σ_{sm}/σ_{DE} at the edges of the temperature range, it can be seen that in the mentioned interval of the values x the metal-insulator transition is realized:

$$\left. \frac{\sigma_{sm}}{\sigma_{DE}} \right|_{x=0.95} \approx \begin{cases} 30 \text{ (50 K)} \\ 12 \cdot 10^{-3} \text{ (6 K)} \end{cases}$$

These ratios clearly demonstrate the simultaneous presence of antiferromagnetic (AFM) and ferromagnetic (FM) phases in the given system. Wherein the metallization is a consequence of the increasing contribution of the FM phase, which reduces the energy of the system, and is the result of self-consistent rearrangement of the corresponding spin configurations AFM \rightarrow FM by free carriers.

Unlike, for example, from narrow-band hole doped four-component perovskite-like structures such as lanthanum manganites, the ESCO system with a smaller width of the e_g multiplet of the d band [74,75] leaves little hope for an outstanding magnetoresistive effect. However, this effect, although not “colossal”, still in some cases can reach tens of percent. There are two characteristic concentration regions where the magnetoresistance effect is significant. This is an area near $x \approx 0.5$ and an area $x > 0.8$, where the most radical changes in the temperature behavior of the conductivity of the samples are observed in the absence of a magnetic field. The important feature of the studying system is the change in the sign of the magnetoresistance during the transitions from one characteristic region x to another and from the range of temperatures T_r to the range T_N in the region $x > 0.8$. Since in “dirty” oxides, which include ceramic specimens, the dynamic properties of the carriers are practically not detected, the observed magnetoresistance effects in perovskites, should reflect the phenomena directly related to the correlation of electronic states as a result of the doping, the temperature change or the applying of a magnetic field, which determine one or another configuration of the magnetic moments of the ions.

It is reasonable to assume that the magnetoresistance in ESCO becomes noticeable ($> 5\%$) in those regions of concentration where the magnetic order undergoes critical

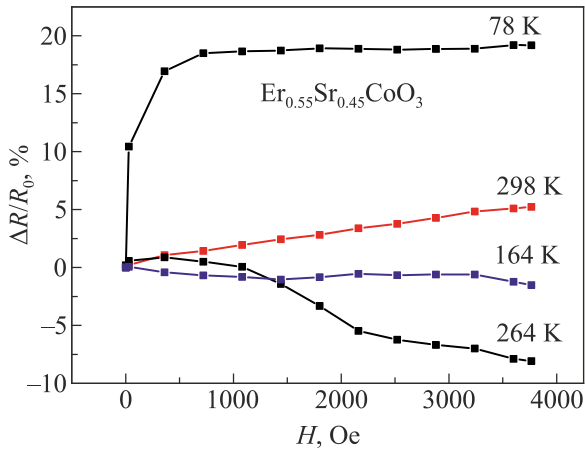


Fig. 12. Field dependencies of the magnetoresistance of the ESCO system with $x = 0.45$ at several temperatures [72].

changes and its character becomes sensitive to the external factors, in particular, to the magnetic fields of insignificant magnitude. This is a good illustration of Fig. 12, which shows the dependences of the magnetoresistance on the magnetic field not higher than 4 kOe for $x = 0.45$. Comparing the behavior of the magnetoresistance in two temperature intervals, T_r (lower curves) and T_N (upper curve), we see that, when T_N , the dependence on the magnetic field has a practically “switching” character: when the field is about 1 kOe, the conductivity falls by almost 17% and then it remains at least 4 kOe, and in the T_r region it smoothly depends on H within the range of 5–7% with a different sign. Such a difference in the behavior of the magnetoresistive effect is possible in the radical distinctions of the character of the magnetic ordering of structures in the regions of T_r and T_N . The same conclusion follows from the concentration dependences of the magnetoresistance.

The most plausible assumption is the presence of the paramagnet \leftrightarrow ferromagnet phase transition in the $\text{Co}^{3+}/\text{Co}^{4+}$

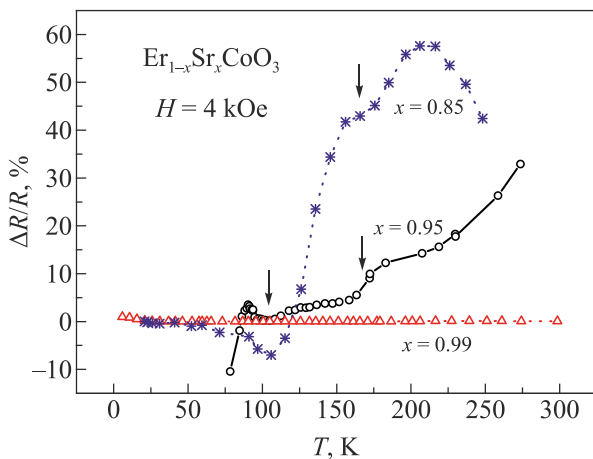


Fig. 13. Temperature dependencies of the magnetoresistance $\Delta R/R_0 = [(R_H/R_0)^{-1}]$ with Sr concentration range $0.85 \leq x \leq 0.99$ in the magnetic field 4 kOe. The probable magnetic phase transitions are marked by arrows [72].

ions system with an ordering temperature $T_c \sim 160$ K, which is estimated from the position of the upper fracture on the curves of the magnetoresistance versus temperature (right arrows in Fig. 13). This assumption is also confirmed by the fact that the greatest value of the magnetoresistance ($\approx 60\%$) obtained at $H = 4$ kOe is achieved precisely with $x = 0.85$. This is that interval of the dopant concentrations, where in the absence of a magnetic field during the transition from $x = 0.85$ to $x = 0.99$ the conductivity radically increase at temperatures below 100 K (Fig. 11). Thus, we can assume that the last effect is related to the phase transition of the AFM \leftrightarrow FM type, which in Fig. 13 is marked by the left lower arrow.

5. Conclusion

This review presents the results of the investigations of the electronic properties of the lanthanum and erbium cobaltites doped with strontium and silver in the wide range of their concentrations. The presence of several phases with different conduction mechanisms is proved, due to strong electron correlations. In particular, in erbium cobaltites an abnormal increase in conductivity and a large magnetoresistance effect in the narrow range of the Sr concentrations ($0.85 \leq x \leq 0.99$) were found, that is associated with the significant role of the double exchange mechanism. In bulk granular lanthanum cobaltites with a granular size of about 1 μm , the transition from metal to nonmetal conductivity with a temperature decreasing is observed. It is shown that this effect is due to the intergranular mechanism of spin-polarized tunneling of the charge carriers between the nearest granules in the conditions of their constant antiferromagnetic exchange interaction.

1. E.L. Nagaev, *Phys. Usp.* **39**, 781 (1996).
2. E.G. Maksimov, *Phys. Usp.* **43**, 965 (2000).
3. M. Imada, A. Fujimori, and Y. Tokura, *Rev. Mod. Phys.* **70**, 1039 (1998).
4. M. Coey, *Nature* **430**, 155 (2004).
5. M.Yu. Kagan and K.I. Kugel', *Phys. Usp.* **44**, 553 (2001).
6. *In Phase Separation in Cuprate Superconductors*, E. Sigmund, K.A. Müller (eds.), Springer-Verlag, Berlin, Germany (1994), p. 401.
7. J. Wu, *PhD Thesis*, University of Minnesota, Twin Cities (2006).
8. M. Dawber, K.M. Rabe, and J.F. Scott, *Rev. Mod. Phys.* **77**, 1083 (2005).
9. V.M. Loktev and Yu.G. Pogorelov, *Fiz. Nizk. Temp.* **26**, 231 (2000) [*Low Temp. Phys.* **26**, 171 (2000)].
10. Yu.A. Izyumov and Yu.N. Skryabin, *Phys. Usp.* **44**, 109 (2001).
11. Y. Long, Y. Kaneko, S. Ishiwata, Y. Taguchi, and Y. Tokura, *J. Phys.: Condens. Matter* **23**, 245601 (2011).
12. N.B. Ivanova, S.G. Ovchinnikov, M.M. Korshunov, I.M. Eremin, and N.V. Kazak, *Phys. Usp.* **179**, 837 (2009).
13. S. Yamaguchi, Y. Okimoto, and Y. Tokura, *Phys. Rev. B* **54**, R11022 (1996).

14. Bernard Raveau and Md. Motin Seikh, *Handbook of Magnetic Materials, Magnetic and Physical Properties of Cobalt Perovskites*, Elsevier (2015), Vol. 23, Ch. 3, p. 161.
15. Y. Kobayashi, T. Mitsunaga, G. Fujinawa, T. Arii, M. Suetake, K. Asai, and J. Harada, *J. Phys. Soc. Jpn.* **69**, 3468 (2000).
16. P. Ravindran, P.A. Korzhavyi, H. Fjellvåg, and A. Kjekshus, *Phys. Rev. B* **60**, 16423 (1999).
17. T. Arima, Y. Tokura, and J.B. Torrance, *Phys. Rev. B* **48**, 17006 (1993).
18. T. Arima and Y. Tokura, *J. Phys. Soc. Jpn.* **64**, 2488 (1995).
19. S. Yamaguchi, Y. Okimoto, H. Taniguchi, and Y. Tokura, *Phys. Rev. B* **53**, R2926 (1996).
20. K. Asai, A. Yoneda, O. Yokokura, J.M. Tranquada, G. Shirane, and K. Kohn, *J. Phys. Soc. Jpn.* **67**, 290 (1998).
21. J. Yan, J. Zhou, and J.B. Goodenough, *Phys. Rev. B* **70**, 014402 (2004).
22. Chao Ma, Nan Lin, Zuyong Wang, Shiming Zhou, Hongchun Yu, Jiangbo Lu, and Hongwen Huang, *Phys. Rev. B* **99**, 115401 (2019).
23. M. Itoh, M. Sugahara, I. Natori, and K. Motoya, *J. Phys. Soc. Jpn.* **64**, 3967 (1995).
24. Y. Tokura, Y. Okimoto, S. Yamaguchi, H. Taniguchi, T. Kimura, and H. Takagi, *Phys. Rev. B* **58**, R1699 (1998).
25. Y. Kobayashi, Y. Sakurai, N. Tsuji, K. Sato, and K. Asai, *Phys. Rev. B* **98**, 115154 (2018).
26. S.R. English, J. Wu, and C. Leighton, *Phys. Rev. B* **65**, 220407 (2002).
27. P.M. Raccah and J.B. Goodenough, *J. Appl. Phys.* **39**, 1209 (1968).
28. D. Louca and J.L. Sarrao, *Phys. Rev. Lett.* **91**, 155501 (2003).
29. D. Phelan, D. Louca, K. Kamazawa, S.-H. Lee, S.N. Ancona, S. Rosenkranz, Y. Motome, M.F. Hundley, J.F. Mitchell, and Y. Moritomo, *Phys. Rev. Lett.* **97**, 235501 (2006).
30. A. Podlesnyak, M. Russina, A. Furrer, A. Alfonsov, E. Vavilova, V. Kataev, B. Büchner, Th. Strässle, E. Pomjakushina, K. Conder, and D.I. Khomskii, *Phys. Rev. Lett.* **101**, 247603 (2008).
31. A. Podlesnyak, G. Ehlers, M. Frontzek, A.S. Sefat, A. Furrer, Th. Strässle, E. Pomjakushina, K. Conder, F. Demmel, and D.I. Khomskii, *Phys. Rev. B* **83**, 134430 (2011).
32. E.L. Nagaev and A.I. Podel'shchikov, *J. Phys.: Condens. Matter* **8**, 5611 (1996).
33. C. He, S. El-Khatib, J. Wu, J.W. Lynn, H. Zheng, J.F. Mitchell, and C. Leighton, *Europhys. Lett.* **87**, 27006 (2009).
34. P.L. Kuhns, M.J.R. Hoch, W.G. Moulton, A.P. Reyes, J. Wu, and C. Leighton, *Phys. Rev. Lett.* **91**, 127202 (2003).
35. M.J.R. Hoch, P.L. Kuhns, W.G. Moulton, A.P. Reyes, J. Lu, J. Wu, and C. Leighton, *Phys. Rev. B* **70**, 174443 (2004).
36. M.J.R. Hoch, P.L. Kuhns, W.G. Moulton, A.P. Reyes, J. Wu, and C. Leighton, *Phys. Rev. B* **69**, 014425 (2004).
37. R.X. Smith, M.J.R. Hoch, P.L. Kuhns, W.G. Moulton, A.P. Reyes, G.S. Boebinger, J. Mitchell, and C. Leighton, *Phys. Rev. B* **78**, 092201 (2008).
38. D. Phelan, D. Louca, S. Rosenkranz, S.-H. Lee, Y. Qiu, P.J. Chupas, R. Osborn, H. Zheng, J.F. Mitchell, J.R.D. Copley, J.L. Sarrao, and Y. Moritomo, *Phys. Rev. Lett.* **96**, 027201 (2006).
39. J. Wu, J.W. Lynn, C.J. Glinka, J. Burley, H. Zheng, J.F. Mitchell, and C. Leighton, *Phys. Rev. Lett.* **94**, 037201 (2005).
40. T. McGuire and R. Potter, *IEEE Trans. Magn.* **11**, 1018 (1975).
41. M.N. Baibich, J.M. Broto, A. Fert, F. Nguyen Van Dau, F. Petroff, P. Etienne, G. Creuzet, A. Friederich, and J. Chazelas, *Phys. Rev. Lett.* **61**, 2472 (1988).
42. W.P. Pratt, Jr., S.-F. Lee, J.M. Slaughter, R. Loloee, P.A. Schroeder, and J. Bass, *Phys. Rev. Lett.* **66**, 3060 (1991).
43. J.Q. Xiao, J.S. Jiang, and C.L. Chien, *Phys. Rev. Lett.* **68**, 3749 (1992).
44. A.E. Berkowitz, J.R. Mitchell, M.J. Carey, A.P. Young, S. Zhang, F.E. Spada, F.T. Parker, A. Hutten, and G. Thomas, *Phys. Rev. Lett.* **68**, 3745 (1992).
45. S. Barzilai, Y. Goldstein, I. Balberg, and J.S. Helman, *Phys. Rev. B* **23**, 1809 (1981).
46. J. Wu, H. Zheng, J.F. Mitchell, and C. Leighton, *Phys. Rev. B* **73**, 020404 (2006).
47. J. Wu and C. Leighton, *Phys. Rev. B* **67**, 174408 (2003).
48. R.X. Smith, M.J.R. Hoch, W.G. Moulton, P.L. Kuhns, A.P. Reyes, G.S. Boebinger, H. Zheng, and J.F. Mitchell, *Phys. Rev. B* **86**, 054428 (2012).
49. M.A. Señaris-Rodríguez and J.B. Goodenough, *J. Solid State Chem.* **118**, 323 (1995).
50. H.Y. Hwang, S. Cheong, N.P. Ong, and B. Batlogg, *Phys. Rev. Lett.* **77**, 2041 (1996).
51. X.W. Li, A. Gupta, G. Xiao, and G.Q. Gong, *Appl. Phys. Lett.* **71**, 1124 (1997).
52. S. Sundar Manoharan, D. Elefant, G. Reiss, and J.B. Goodenough, *Appl. Phys. Lett.* **72**, 984 (1998).
53. J.M.D. Coey, A.E. Berkowitz, L.I. Balcells, F.F. Putris, and F.T. Parker, *Appl. Phys. Lett.* **72**, 734 (1998).
54. Yu.N. Chiang, M.O. Dzyuba, O.G. Shevchenko, A.A. Kozlovskii, and V.F. Khirnyi, *J. Mod. Phys.* **1**, 319 (2010).
55. Yu.N. Chiang, M.O. Dzyuba, O.G. Shevchenko, and V.F. Khirnyi, *Fiz. Nizk. Temp.* **38**, 76 (2012) [*Low Temp. Phys.* **38**, 59 (2012)].
56. S. Enache, M. Dragan, M. Varlam, and K. Petrov, *Materials* **12**, No. 15, 2359 (2019).
57. B.I. Belevtsev, N.T. Cherpak, I.N. Chukanova, A.I. Gubin, V.B. Krasovitsky, and A.A. Lavrinovich, *J. Phys.: Condens. Matter* **14**, 2591 (2002).
58. C. Zener, *Phys. Rev.* **82**, 403 (1951).
59. P. Friš, D. Munzar, O. Caha, and A. Dubroka, *Phys. Rev. B* **97**, 045137 (2018).
60. P. Sheng, B. Abeles, and Y. Arie, *Phys. Rev. Lett.* **31**, 44 (1973).
61. J.S. Helman and B. Abeles, *Phys. Rev. Lett.* **37**, 1429 (1976).
62. P. Raychaudhuri, K. Sheshadri, P. Taneja, S. Bandyopadhyay, P. Ayyub, A.K. Nigam, R. Pinto, Sujeet Chaudhary, and S.B. Roy, *Phys. Rev. B* **59**, 13919 (1999).
63. A.E. Kar'kin, D.A. Shulyatev, A.A. Arsenov, V.A. Cherepanov, and E.A. Filonova, *J. Exp. Theor. Phys.* **89**, 358 (1999).
64. E. Rozenberg, M. Auslender, I. Felner, and G. Gorodetsky, *J. Appl. Phys.* **88**, 2578 (2000).
65. M.I. Auslender, E. Rozenberg, A.E. Kar'kin, B.K. Chaudhuri, and G. Gorodetsky, *J. Alloys Compd.* **326**, 81 (2001).

66. N. Zhang, F. Wang, W. Zhong, and W. Ding, *J. Phys.: Condens. Matter* **11**, 2625 (1999).
67. N. Zhang, W. Ding, W. Zhong, D. Xing, and Y. Du, *Phys. Rev. B* **56**, 8138 (1997).
68. O. Ciftja, M. Luban, M. Auslender, and J.H. Luscombe, *Phys. Rev. B* **60**, 10122 (1999).
69. X. Liu and C.T. Prewitt, *J. Phys. Chem. Solids* **52**, 441 (1991).
70. P.G. Radaelli and S.-W. Cheong, *Phys. Rev. B* **66**, 094408 (2002).
71. Yu.N. Chiang, V.F. Khirnyĭ, O.G. Shevchenko, A.A. Kozlovskii, A.V. Semenov, V.M. Puzikov, and T.G. Deĭneka, *Fiz. Nizk. Temp.* **34**, 1197 (2008) [*Low Temp. Phys.* **34**, 947 (2008)].
72. Yu.N. Chiang, M.O. Dzyuba, V.F. Khirnyĭ, O.G. Shevchenko, and A.A. Kozlovskii, *Fiz. Nizk. Temp.* **35**, 1123 (2009) [*Low Temp. Phys.* **35**, 876 (2009)].
73. J. Padilla-Pantoja, J.L. García-Muñoz, J.A. Alonso, and M.T. Fernández-Díaz, *J. Phys.: Conf. Ser.* **663**, 012005 (2015).
74. I.A. Nekrasov, S.V. Streltsov, M.A. Korotin, and V.I. Anisimov, *Phys. Rev. B* **68**, 235113 (2003).
75. A. Abragam and B. Bleaney, *Electron Paramagnetic Resonance of Transition Ions*, Clarendon Press, Oxford (1970), p. 700.

Электрический транспорт в кобальтитах лантана и эрбия (Обзор)

Ю.Н. Цзян, М.О. Дзюба

Обзор посвящен проводящим свойствам многоэлементных соединений, таких как лантановые и эрбиевые кобальтиты. Эти свойства связаны с контролируемым легированием взаимодействием делокализованных электронов с локальными магнитными моментами. Рассмотрены основные физические механизмы, определяющие транспортные свойства перовскитоподобных материалов. Приведены основные экспериментальные результаты для кобальтитов лантана и эрбия. Рассмотрено влияние фактора поликристалличности образцов на их гальваномагнитные свойства.

Ключевые слова: гранулированный кобальтит, магнитосопротивление, двойной обмен, спин-поляризованное туннелирование.

Електричний транспорт у кобальтитах лантану та ербію (Огляд)

Ю.М. Цзян, М.О. Дзюба

Огляд присвячено провідним властивостям багатоелементних з'єднань, таких як лантанові та ербієві кобальтити. Ці властивості пов'язані з контрольованою легуванням взаємодією делокалізованих електронів з локальними магнітними моментами. Розглянуто основні фізичні механізми, що визначають транспортні властивості перовськітоподібних матеріалів. Наведено основні експериментальні результати для кобальтитів лантану та ербію. Розглянуто вплив фактору полікристалічності зразків на їх гальваномагнітні властивості.

Ключові слова: гранульований кобальтит, магнітоопір, подвійний обмін, спин-поляризоване тунелювання.